

Optimum Control of Flow around a Circular Cylinder with Non-Uniform Suction

James Ramsay¹, Mathieu Sellier^{1 a)}, Wei Hua Ho²

¹*Department of Mechanical Engineering, University of Canterbury, Christchurch, New Zealand*

²*Department of Mechanical and Industrial Engineering, University of South Africa, Pretoria, South Africa*

a) Corresponding author: mathieu.sellier@canterbury.ac.nz

Abstract. In the present study, numerical investigations were performed to determine the optimum non-uniform suction profiles to control the flow around a circular cylinder in the range of Reynolds numbers $4 < Re < 200$. To investigate how the characteristics of the optimal control and the resulting flow change depending on the optimisation objective, several objectives were explored, namely: minimising the separation angle, total drag, and pressure drag. A variety of suction control implementations were investigated and compared to the performance of uniform suction. It was determined that the optimal non-uniform suction profiles consisted of a distribution with compact support, and a single locus. The location of the optimum suction region and the amount of suction necessary to achieve each objective varied substantially with Reynolds number, but with a predictable relationship. It is also shown that these parameters can alternatively be considered as related to the separation angle of the uncontrolled flow (the initial separation angle). Depending on the objective, the control parameters varied greatly: less suction was necessary to minimise total drag than to eliminate separation. Non-uniform suction profiles were much more efficient at eliminating boundary layer separation, requiring the removal of less than half the volume of fluid as uniform control to achieve the same objective. Total elimination of boundary layer separation did not always result in an improvement in total drag, and in some circumstances increased it. An analysis of the drag components showed that, although the pressure drag was substantially improved by boundary layer suction, the disappearance of the separated region downstream resulted in faster flow over the cylinder and consequently a higher skin friction drag. The drag-optimised flows had characteristics very close to those of a steady cylinder within the unsteady regime. These results show that the balance of drag components must be an important consideration when designing flow control systems and that, when done appropriately, substantial improvement can be seen in the flow characteristics.

INTRODUCTION

The flow around a circular cylinder has been the subject of much interest for over a century and, for almost as long, so has the problem of controlling it. This bluff body flow can produce high drag and lift characteristics as well as a variety of undesirable flow phenomena – especially vortex shedding. To complicate the search for optimal control parameters, the behaviour of the flow and its impact on the aerodynamic characteristics of the cylinder vary widely with relatively small changes in Reynolds number ($Re = \frac{\rho UD}{\mu}$). Although much focus has been paid to minimising the drag or eliminating vortex shedding by flow control, the phenomenon of boundary layer separation – which plays an important role in the arising of both these features – has not attracted as much scrutiny. Despite the sustained interest in this field, the problem of optimal control for this flow is a matter that is far from settled.

The flow around a circular cylinder offers a complex problem for the study of flow control because the features of the flow can be changed substantially only by varying the Reynolds number. In the range of Reynolds numbers from 10^0 to 10^7 , Williamson¹ distinguishes the resulting flows into nine regimes with unique features and phenomena. Zdravkovich² divides them more finely, with four additional regimes. At low Re , the flow is unseparated and steady ($Re < 6$), but in the range of $6 < Re < 47$ the boundary layer separates and a pair of vortices form behind the cylinder; the separation point moves toward the front of the cylinder with increasing Re . At about $Re = 47$, the well-known phenomenon of vortex shedding begins and continues in a two-dimensional manner up until $Re = 188.5$ where the

vortex shedding begins to exhibit 3D features. With further increasing Re the wake becomes even more complex as different areas of the flow transition to turbulence, beginning with the wake, moving up the shear layers, and finally transitioning in the boundary layer, which marks the onset of the well-known ‘drag crisis’. At this point, the separation point is delayed significantly, jumping much further aft and providing a substantial decrease in pressure drag. Clearly, any attempt to provide optimal flow control over this entire range would be exceedingly difficult if not impossible. However, by investigating small regions of the Re range, relationships between the flow and control parameters can be established which may shed light on other regimes (or to entirely different body-fluid flows). Much research has been performed on the cylinder at high Re , particularly near the critical point $Re \approx 2 \times 10^5$ (sub-critical regime), because many engineering situations in real life experience such conditions. For investigating the physics of flow control, though, the low Re range offers the best conditions. The small range of $Re < 200$, which was used for this study, includes three very different flow regimes with major shifts in phenomena. The flow remains fully laminar and two-dimensional over the entire range, though, which means it can be easily modelled and experimented upon.

One of the important features of bluff body flows is the separation angle, θ_s , which marks the point where the boundary layer separates from the surface as measured from the leading or trailing edge of the body (trailing edge for this paper). It is commonly held that once the boundary layer has separated and become sufficiently established, the separation angle does not change significantly until the drag crisis at $Re \approx 2 \times 10^5$ where it jumps from about 100° to 60° ^{3,4}. Unfortunately, this parameter has not been considered to be a particularly important feature for measurement or control. In many papers exploring the flow around circular cylinders, the separation angle is only described as a variable of secondary importance – usually only in discussion of the features of the pressure profiles. In actuality, however, the separation angle is in many ways the key mover of the flow phenomena, not their object. The pressure drag, C_{d_p} , which makes up almost all of the total drag on the cylinder at high Re is predominantly caused by the separation of the boundary layer. Vortex shedding occurs when vortical structures developed in the shear layers grow from the surface. Furthermore, experiments over a wide Re range by Weidman⁵, and separately by Achenbach⁶, show that the separation angle is a more active feature than commonly held, perpetually moving across the entire Re range, and not always monotonically.

In 2004 Wu et al.⁷ performed a review of experiments which had measured the separation angle of the cylinder at low Re , and found that the results between studies deviated by as much as 10° . By their own experimentation and numerical simulation, the researchers found accurate values and determined the causes of the deviation – mostly due to different measurement techniques. This demonstrates one of the many reasons that the separation angle has been relatively unexplored in the literature – difficulty in measuring it accurately. An approximation that the separation point corresponds to the inflection point of the pressure curve over the cylinder is commonly used, as by Fransson et al.⁸, but may not be entirely accurate. However, the improvement of experimental techniques and equipment has now eliminated many of these problems, and these difficulties are not present in computational fluid dynamics (CFD). Therefore, there is no reason that the separation angle should not be a feature of particular interest – both in terms of its importance in the arising of other phenomena like vortex shedding, but also as a parameter that itself might be directly controlled.

To date, many active and passive methods of control have been investigated to control the flow around the circular cylinder. These range from simple geometric features such as splitter plates⁹ and helical strakes¹⁰ to complex active measures like plasma actuators¹¹ or magnetic fields¹². Many of these are described in the Annual Review by Choi, Jeon and Kim¹³ or in a 2016 review by Rashidi et al.¹⁴ Each of these methods have achieved some success at reducing drag or weakening vortex shedding, though often at significant cost. One of the simplest forms of flow control is boundary layer suction. This method removes the low momentum fluid particles at the surface, thus entraining higher momentum particles from the free-stream to reinvigorate the boundary layer, and delaying separation. This method of flow control is as old as the boundary layer concept itself – with Prandtl testing his theory by experimenting on slot suction of a cylinder¹⁵. Nevertheless, it is still not a settled matter how this method can optimally control the flow around a circular cylinder, i.e. achieve the control objective with the least suction/fluid removal. Boundary layer suction has many advantages compared to other control methods. For one, the geometry of the body does not have to be changed (although the materials of the surface may have to). Further, the method is simple and practical – its parameters can be adjusted easily and have a wide range; there is no multi-physicality to this control. And of particular importance to this study, the method is well researched both experimentally and numerically, but there is no clear consensus on its optimal parameters.

Experiments on suction control began in the early 20th Century, and much interest was paid to this subject for the improvement of aerodynamic characteristics for aircraft during the Second World War¹⁶. Over this time, two main applications of suction control were investigated: uniform suction over the entire surface of a cylinder with porous

walls – as researched experimentally by Thwaites and his colleagues^{17,18} – and slot suction, where only part of the boundary layer is removed through a slot or series of slots in the cylinder surface. Pankhurst and Thwaites¹⁷ found that sufficient uniform suction resulted in the flow approaching that seen for potential flow, with improvements in drag and elimination of vortex shedding. More recently, Fransson et al.⁸ determined a relationship between the controlled flow using uniform suction on the cylinder and the uncontrolled flow at a different Reynolds number, and that these could be linked via the Strouhal number. However, the effective Reynolds relationship found by Fransson et al. is only applicable if the control does not entirely suppress vortex shedding which is a common objective for bluff body flow control. Uniform suction has its disadvantages, namely the inefficiency of removing material at all areas of the cylinder – even where it may not be necessary – and its limited control parameters. Slot suction is similarly disadvantaged, being limited in its location of application, the distribution profile of the suction, and the discontinuity of its nature. A study of distributed slot suction (varying in the spanwise direction) by Kim and Choi¹⁹ found that the objective of control (total drag in this case) was very sensitive to the location of the slots, and at $Re = 100$ the best results were achieved with the slots located between $80-100^\circ$.

A better approach to suction control combines the benefits of each of these methods – non-uniform suction. This method is applied similarly to uniform suction by using a porous surface, however the suction is applied unevenly, with the possibility of any potential distribution over the surface – continuous or otherwise. Theoretically, this allows much more precise control of the flow, with the possibility to concentrate the suction control at critical areas of the surface and apply no control where it is unnecessary. Because there are so many potential profiles for this method, determining its “optimum” is not straightforward. Some papers on this subject have been published, particularly with the focus of utilising it in conjunction with feedback from the flow in order to mitigate the wide-range of potential implementations. Min and Choi²⁰ employed sub-optimal feedback to control the parameters for non-uniform suction and blowing. The researchers successfully reduced the pressure drag of the surface, and achieved pressure profiles closer to those predicted by potential flow theory. However, as the focus of this study was the development of sub-optimal feedback using limited time-steps of control, this paper only offers an introduction to what the true optimal control might look like with this method. Li et al. performed a similar numerical experiment and carried out a complete adjoint optimisation procedure with unsteady, time-dependent simulations. The researchers achieved a complete control of vortex shedding for up to $Re = 110$. They also found that the optimal controls were insensitive to initial conditions if the control was applied for time-scales longer than the vortex shedding period. The researchers used objectives for the error between the flow field and potential flow field, the enstrophy of the flow (to suppress vortex shedding), and the minimisation of drag. The separation angle of the flow was not investigated. Very recently, the optimum spanwise-varying suction/blowing control of a 3D circular cylinder in 2D flow was determined using eigenmode analysis by Boujo et al.²¹ Due to the nature of this method, though, it can only be used to optimise for stabilisation or frequency modification which does not necessarily coincide with minimised drag. All of these studies were performed by numerical methods; non-uniform suction has not been explored substantially by physical experimentation.

These studies suggest that non-uniform suction offers a control method that can be used to optimally achieve a variety of objectives for the flow around circular cylinders. Despite this interest though, the optimal profiles for this type of control are not clear, nor has a comparison with the other implementations of suction control (uniform and slot suction) been performed to any depth. Throughout most investigations into the control of flow around a circular cylinder, the importance and impact of the separation angle appears to have been under-investigated. Therefore, the objective of the present study is to comprehensively investigate the variety of suction control methods for a circular cylinder by numerical investigation, with particular focus on the separation angle as an output parameter and control objective. A variety of optimisation studies with differing setups and objectives were performed in the Reynolds range of $4 < Re < 200$ in order to best determine the relationships between the three factors of control – uncontrolled flow, control parameters, and the resulting flow. This Re range offers a variety of flow regimes (unseparated flow, separated steady flow, and vortex shedding) while offering a simple, two-dimensional and fully laminar flow to carry out many simulations. Of particular interest were the impacts of different control setups and objectives on the features of separation angle, drag components, pressure profiles, and the general features of the flow.

METHODS AND MODELLING

Geometry, mesh and solver methods

The governing equations for unsteady incompressible and isothermal viscous flow are described by the following:

$$\frac{\partial u_i}{\partial t} + u_j \frac{\partial u_i}{\partial x_j} = -\frac{\partial p}{\partial x_i} + \frac{1}{Re} \frac{\partial^2 u_i}{\partial x_j \partial x_j},$$

$$\frac{\partial u_i}{\partial x_i} = 0,$$

where u_i represents the velocity components, x_i gives the directional vectors, and p is the pressure. For some of the simulations, the flow was modelled as steady, and so the time derivatives vanished. The laminar flow module of COMSOL Multiphysics was used to solve the system for all the studies in the present investigation. Fluid properties for water at 20°C were used for the model, employing the above equations. For the time-dependent cases, an implicit time-stepping method was employed with ‘Intermediate’ stepping to reduce the CFL restrictions while preventing numerical smearing and enabling the instabilities that induce vortex shedding. A time-step giving 30 steps per vortex shedding period resulted in accurate and sufficiently precise results for the mesh described in Figure 1 and Table I. With this time-step, dt is defined as $dt = \frac{1}{30} T = \frac{1}{30} \frac{D}{U St}$, where St is the Strouhal number and T the period of vortex shedding, $St = \frac{D}{TU}$ and is equal to $St = 0.212 - \frac{5.4}{Re}$ in the range investigated here. The computational domain and mesh are shown in Figure 1. This domain was based on that employed successfully by Wu et al.⁷

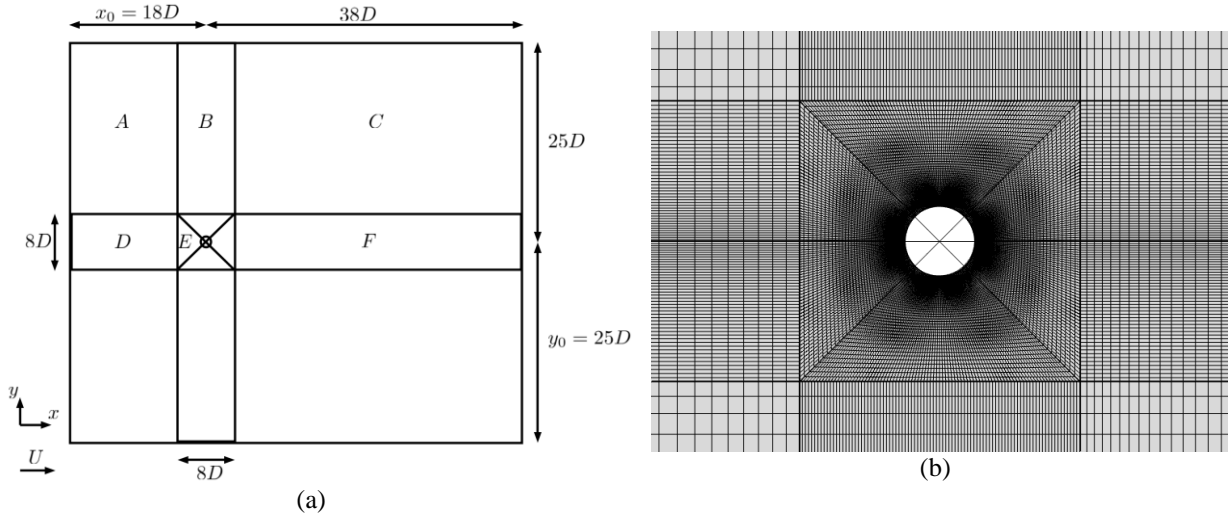


Figure 1: Sketch of (a) computational domain and (b) close-up view of element mesh around the cylinder

The inlet (left-boundary) was assigned a uniform flow boundary condition with velocity, $u = U = \frac{Re v}{D}$, $v = 0$. The upper and lower boundaries were modelled as no-slip moving walls with the same velocity profile as the inlet. This minimises any potential blockage effects that may result from the artificially limited domain. The actual domain has blockage ratio, $BR = \frac{1}{50} = 0.02$ which was shown to reduce the error in measured separation angle to below 0.2% by Wu et al. A pressure outlet condition was imposed on the outlet (right-boundary) with zero relative pressure. The cylinder walls were modelled as a fixed-velocity outlet with defined normal outflow velocity, $u_n = v_w$, $u_t = 0$, where u_n and u_t are the normal and tangential velocity components at the wall, respectively. This boundary condition made it possible to define any suction or blowing profile on the cylinder wall by only changing the function that defines v_w , the suction velocity. In keeping with the terminology typically used in the literature, the non-dimensional suction coefficient, $c_q = \frac{v_w}{U} \times 100$, was used as the control parameter, from which v_w was defined. In this paper c_q with a lower case ‘c’ refers to the local suction coefficient at any particular point on the cylinder, while C_q refers to the global

suction coefficient of the cylinder as a whole, $C_q = \frac{1}{2\pi} \oint c_q d\theta$. The two definitions will be useful given that non-homogeneous suction profiles are the subject of this investigation. With this boundary condition, locations where no suction is applied have the same definition as a no-slip wall.

Table I: Characteristics of mesh found to be independent for steady-state and transient solutions.

Region	Number of Grid Points (x × y)	Number of Elements	Average Quality	Minimum Quality
A	20x20	400	1.000	1.000
B	80x20	1600	1.000	1.000
C	20x60	1200	1.000	1.000
D	20x80	1600	1.000	1.000
E	45x98	4410	0.843	0.500
F	60x80	4800	1.000	1.000
Total		31640	0.904	0.500

Suction control setup

One of the objectives of this study was to investigate how non-uniform suction profiles might more efficiently control the flow around the circular cylinder than uniform suction. To explore this, three methods for applying non-uniform suction profiles were devised. These are summarised in Figure 3. The values underneath each setup show the number of control parameters for each distribution. Since a theoretically infinite variety of non-uniform suction profiles might be generated, and since it was desirable to be able to model any shape of these profiles, the six-segment profile was employed. Of the potential suction profiles, these may be divided into two categories: those with one locus of suction and those with multiple. The six-segment control method can model both. For this setup, the cylinder is divided into twelve equal segments and the suction coefficient at the centre of each is used as the control variables, c_{qn} . As we were not concerned with the lift or lateral forces of the cylinder, the lower half segments were set to mirror the upper half, so there were only six segments for control. To create a continuous suction profile from the six discrete values, pointwise interpolation with a continuous second-derivative constraint was applied. In this way, a suction profile with multiple loci of suction could be modelled. Preliminary investigations found that six-segment control, as opposed to using more or less segments, gave the best control at a Reynolds number of 180.

Preliminary investigations also found that the optimal suction profiles typically had only one locus of suction. The “moving distribution” was defined to generate this type of distribution using fewer parameters. Here three control parameters are used: the maximum local suction coefficient, c_{qmax} , location of suction, θ_q , and spread of suction, γ_q . To create a smooth suction profile, a cubic curve was defined from these parameters and the condition of zero-gradient was applied at the edges and centre of the profile. Thus, a distribution with compact support can be generated, and by changing the θ_q parameter, it can be moved over the cylinder surface. The flexi-moving distribution was identical to the moving distribution profile except for the addition of a fourth control parameter: a bias factor, λ_q . This allowed the suction profile to be asymmetrical, though it introduces the risk of a profile that is so steep it creates separation bubbles in the flow. In addition to these non-uniform suction profiles, uniform suction was also investigated. Here, only one parameter was necessary, c_q , which was held constant at all locations on the cylinder surface.

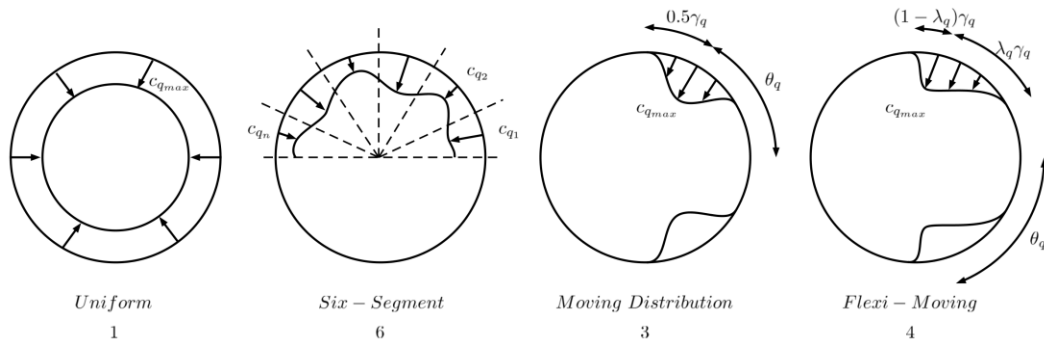


Figure 2: Schematic of the types of control methods investigated.

Optimisation methods

To best understand how the optimal flow control changes depending on the objective of the control, three different cost functionals were defined for the present study:

$$J_1 = \theta_s = \theta \left(u_t|_{r=1.001R} = 0, \frac{-\partial u_t}{\partial \theta} < 0 \right) \quad (1)$$

$$J_2 = C_{d_t} = C_{d_p} + C_{d_f} = \frac{2}{\rho U^2 D} \oint \left(-p(\theta)|_{r=R} + \mu \frac{-\partial u_t(\theta)}{\partial r} \Big|_{r=R} \right) \cos(\theta) R d\theta \quad (2)$$

$$J_3 = C_{d_p} = \frac{2}{\rho U^2 D} \oint -p(\theta)|_{r=R} \cos(\theta) R d\theta \quad (3)$$

J_1 is the angle of separation as measured from the trailing edge. For this study, the separation point was located by determining where the flow reverses direction very near to the wall (measured along a curve with a diameter of $1.002D$). In some cases, such as in the unsteady vortex shedding regime, there are several points of separation and reattachment. The angle of separation we are concerned with is that for the first point of separation, i.e. that closest to the front stagnation point (the leading edge, LE). This identification was carried out using a custom MATLAB function that was implemented into the COMSOL model. It was verified by comparison to the point that the skin friction drag reduces to zero, another feature of separation points. Control that prevents separation will minimise J_1 asymptotically to zero as the separation point reaches the trailing edge.

J_2 is the total drag coefficient, C_{d_t} – the sum of the pressure drag, C_{d_p} , and skin friction drag, C_{d_f} , coefficients. The total drag of the uncontrolled cylinder is quite non-linear in relation to Re so we would not expect the prevention of separation to necessarily correspond to a minimisation of drag due to the several impacting factors contributing to this force.

J_3 is the pressure drag. It is typically assumed that the pressure drag arises solely from the separation of the boundary layer. The loss of momentum to the vortical structures that form as a consequence means that the pressure is not fully recovered on the lee side of the body. However, pressure drag can arise even in an unseparated flow as there is still momentum lost through the no-slip interaction with the wall. Because of this, the minimisation of pressure drag was investigated as its own objective to see how it compares to the separation objective results, J_1 .

In addition to these three, an additional objective was included in each of the studies. The optimal suction control was defined for this study as that which would achieve the objective with least effort, therefore a secondary objective is necessary to measure the controller effort, i.e. the net suction. This objective is defined as the cost function, J_w , below. The overall cost functional for the studies investigated here, is therefore the sum of J_w and J_n (where J_n is one of J_1 , J_2 or J_3 dependent on the present study). As the efficiency of control is of secondary concern to achieving the actual flow characteristic objective, a scaling factor of 0.01 was employed in the addition of J_w to the global objective as shown in Equation 5.

$$J_w = C_q = \frac{1}{2\pi} \oint c_q(\theta) d\theta \quad (4)$$

$$J_{global} = J_n + \frac{1}{100} J_w \quad (5)$$

The ‘Optimization Module’ of COMSOL Multiphysics includes several optimisation methods that can be used to solve problems such as those presented here. In earlier investigations, the Coordinate Search (CO) method had been used to some success, however it is very sensitive to the number of parameters and their order. The Nelder-Mead²² (NM) method, on the other hand, was less sensitive to the parameter order though often taking much longer to converge to a final solution. It was less likely to converge to a local minimum instead of the global, however. In this investigation, both methods were used at different times. For the separation angle objective with the six-segment control a variety of the methods were tested, as well as a variety of orderings for the control parameters. For the drag objectives, however, the NM method was used almost exclusively as it was the most robust, and for the moving distribution setup – with only a few parameters – it was not too slow. Here, the typical optimisation process required about 100 iterations, and could take between 20-40 minutes total depending on the Reynolds number. Each iteration consists of solving the steady-state flow for the input parameters, evaluating the objective function, and adjusting the control parameters for the next iteration. In this paper, where a study has been repeated with different optimisation methods or parameter ordering, the best results will be shown, except where comparisons between the methods/setup are made.

RESULTS

Validation of model

The model was validated by comparing the measured separation angles for the uncontrolled flows to those found in experiments and other numerical studies, as reviewed by Wu et al⁷. This is shown in Figure 3 (a). It can be seen in this figure, that the time-dependent simulations model the flow accurately – the instantaneous behaviour is accurate too, although these values from the literature are not shown in the plot. The steady-state results diverge from the expected values within the vortex shedding regime ($Re > 47$). These values do follow the same trend as the actual behaviour, however, and result in earlier separation angles so provide a conservative approximation. Since it is known that sufficient boundary layer suction stabilises an unsteady flow, and it is anticipated that a control that eliminates boundary layer separation will necessarily be stable, it was decided that the steady-state solver would be satisfactory for the optimisation process. This assumption may follow for the separation angle objective, but the final state of the controlled flow is less well-defined for the drag objectives, and therefore the results may not be as accurate. For this reason, time-dependent simulations were also used to validate the optimal results for each objective. As will be discussed later, this assumption of steady flow, indeed, was not accurate for the drag objectives at all Re .

In this study, the aerodynamic characteristics of the cylinder are of particular interest, therefore it was necessary to validate the measurements of the drag components also. Again, this was carried out by comparing the uncontrolled flow from time-dependent simulations with historical data^{23–25}. These results are shown in Figure 3 (b) and show a good fit. The data from Wieselsberger²⁵ and Tritton²³ come from physical experiments, while the results from Henderson are from direct numerical simulations (DNS). The values from Henderson are used as the benchmark in this paper as the author provided good fits to his data. They are limited, however, in that Henderson only modelled the cylinder at $Re > 25$ so the fits may not be valid for the steady regimes.

Again, in the vortex shedding regime, the steady-state model diverges from the actual values. It is important to note that the steady solver underestimates the drag, despite the separation angle being determined to be closer to the leading edge of the cylinder. One might have expected the pressure drag, and therefore the total drag, to be larger with an earlier separation angle but that is not the case here. Without the modelling of the unsteady vortices and the large lateral movements in the wake, the effects on the pressure and drag are not appropriately captured.

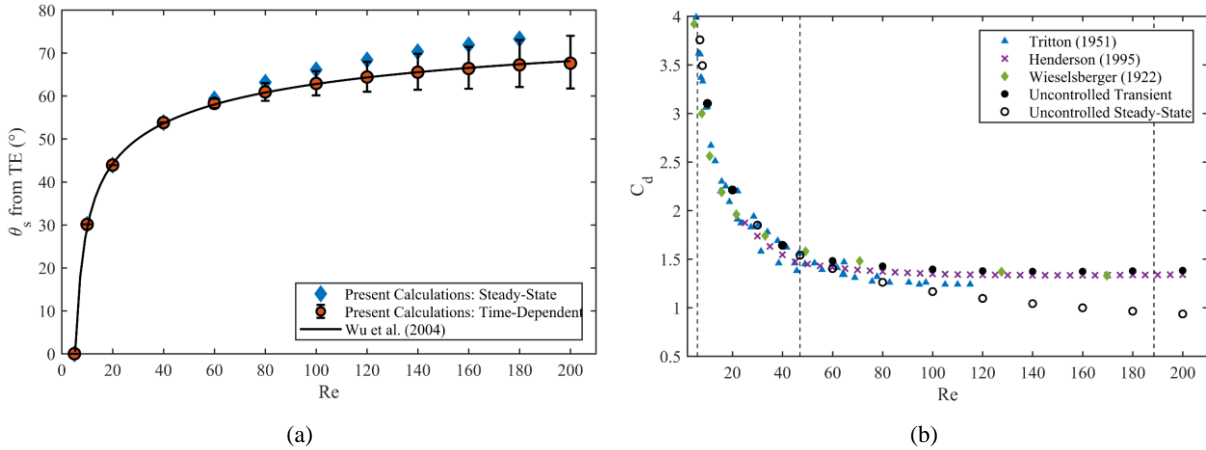


Figure 3: Validation of model by comparison to historical data for (a) the separation angle and (b) the time-averaged total drag coefficient. Here, the error-bars indicate the span of instantaneous values, while the points are time-averaged values.

Separation objective

In this section, we present results from the optimisation studies with the objective of minimising the separation angle, J_1 . We investigate the effectiveness of each suction control setup, with particular focus on the total suction coefficient, C_q , the location of suction, θ_q , the effect on drag and its components, and the pressure profile over the cylinder with and without control.

A. Best control methods

For all control setups, the objective of eliminating boundary layer separation was successfully achieved. A sample of the resulting flows can be seen in Figure 4 along with the instantaneous flow field of the uncontrolled case for comparison. It can be seen in these figures that the controlled flows all have a similar structure, with a much smaller, symmetrical wake. The streamlines illustrate how the freestream fluid is entrained as it passes the cylinder to replace the fluid removed through the suctioned surface. An important feature to note is that the velocity vectors near the top and bottom of the cylinder are much larger in the controlled cases. This is because there is no longer stagnated and separated flow downstream, so the fluid can flow more quickly over the cylinder – more like potential flow. This may be necessary for eliminating separation, but it can have adverse effects on the drag characteristics.

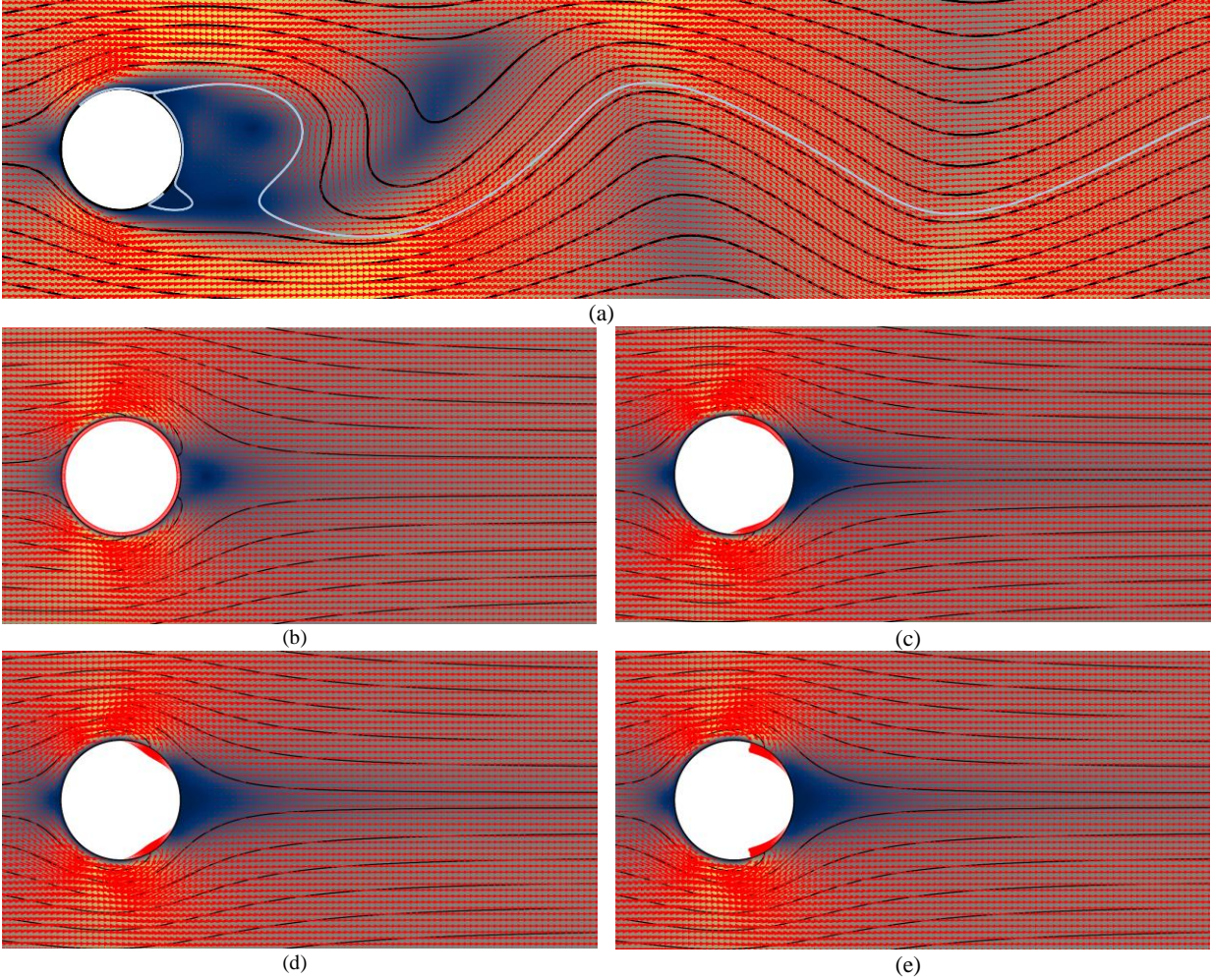


Figure 4: Instantaneous flow fields for controlling separation angle at $Re = 120$: (a) uncontrolled case, (b) uniform suction, (c) six-segment control, (d) moving distribution, and (e) flexi-moving distribution. The streamlines, velocity vectors, and velocity surface are shown. The paler streamline in (a) originates on the curve used for detecting the separation angle.

It may be difficult to tell by the flow fields in Figure 4 alone that the amount of suction required to eliminate separation is much greater for the uniform case than the non-uniform methods of control. The plots in Figure 5 show the suction quantity coefficient, C_q , against the Reynolds number and the initial separation angle before control is applied. It is clear from this figure that uniform suction requires much more control effort to eliminate separation compared to any of the other methods. In all instances (except the trivial non-separated cases), the control effort is at least twice that of the non-uniform suction.

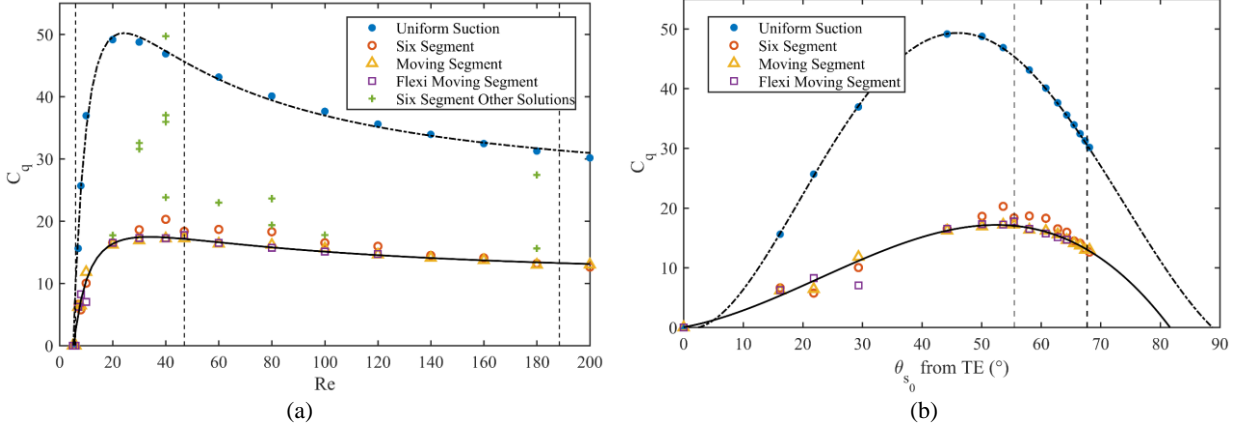


Figure 5: Global suction coefficient for optimal control to prevent separation plotted against (a) the Reynolds number, (b) the separation angle of the uncontrolled flow. The dashed vertical lines indicate regime changes of the uncontrolled flow.

These plots show interesting features regarding the relationship between the flow features and the necessary control effort. For all methods, the amount of suction required to eliminate separation increases in the vortex-pair regime ($Re < 47$) up to a point, after which it decreases with increasing Re . Figure 5 (a) provides rational fits for the uniform and moving distribution data each with a 2nd degree numerator and denominator. For the relationships with the initial separation angle in Figure 5 (b), polynomial fits were more appropriate. It is important to note that these are only fits for the data, and there is no physical justification for their form or parameter values. Nevertheless, clear trends can be seen between the uncontrolled flow features and the necessary control parameters. Extrapolating these trends to higher Reynolds numbers suggests that the suction control effort would plateau near $C_q = 23$ and $C_q = 10$ for uniform and moving distribution suction respectively. However, given what we know of the uncontrolled flow, and how substantially the characteristics of the flow change with increasing Re alone, it may be unreasonable to try and apply these formulae outside the regimes they were tested on. Pankhurst & Thwaites¹⁷ found that a suction quantity of $C_q \sqrt{Re} \geq \frac{30}{\pi}$, was required to eliminate separation on a cylinder fitted with a splitter plate in the Re range of $10^4 - 10^5$. Extrapolating the present results to this regime, a suction coefficient of $C_q \sqrt{Re} \approx \frac{14}{\pi}$ is necessary^a. Likewise, Pankhurst & Thwaites' relationship cannot be extended to the present regime, $Re < 200$, as it would suggest a suction coefficient of $C_q = 150.9$ would be necessary at $Re = 40$ which is obviously not the case. The Reynolds number does not contain sufficient information about the drastic changes in flow features to allow for these relationships to be extended.

On the other hand, the separation angle is a feature of the uncontrolled flow that itself is altered with the regime changes. Since, there is a clear trend between the uncontrolled separation angle, θ_{s_0} , and the required control – and given the uncontrolled separation angle reflects the conditions of the flow regime – it may be possible to extend the relationship with θ_{s_0} into higher Re ranges. After all, the mechanism by which the suction reinvigorates the boundary layer should also remain the same whenever the boundary layer and the shear layers directly adjacent to it are still laminar, in other words, almost up to the transition to turbulence at $Re \approx 2 \times 10^5$.

It can be seen in Figure 5 that the best results are usually achieved with the flexi-moving distribution. The improvement in C_q compared to the moving distribution profile is marginal though – a maximum difference of 40% at $Re = 10$, but less than 3% at all higher Re , and in some instances the moving distribution giving a better result ($Re = 80, 100$). Furthermore, the flexi-moving distribution has potential issues with discontinuities in the model due to the steep suction profiles it can generate (as seen at $Re = 120$ in Figure 4). Finally, as discussed earlier, the optimisation process is most stable for setups with the least number of control parameters. Therefore, since there seems to be little advantage in using the more complex flexi-moving distribution over its symmetrical variety, the rest of the results will be concerned with the moving distribution profiles only.

^a Pankhurst & Thwaites defined C_q as the flow rate through the porous wall divided by (UD) , i.e. $C_q = \frac{v_w}{U} \pi$ according to our notation, hence the introduction of the π term to their equation in this text.

Figure 5 (a) demonstrates how important the appropriate setup of control parameters and optimisation methods are. The ‘Other Solutions’ shown for the six-segment setup were mostly generated when the Coordinate Search method was employed, with differing orders of control parameters. Some of these solutions were generated when testing other optimisation methods such as BOBYQA²⁶ or Nelder-Mead²². The sensitivity to the optimisation setup was particularly high near the regime change at $Re = 47$. These solutions highlight one of the major downsides of using optimisation procedures: the convergence to local minima instead of the global minimum for the objective functional. With carefully selected methods and appropriate setups, however, this risk can be minimised. Reducing the number of independent control parameters reduces the chance of convergence to a local minimum. Similar tests of different methods and parameter orders for the other control setups (moving and flexi-moving distributions) did not generate such divergent results.

B. Optimal suction profiles

An interesting result from the optimisation studies for this objective was how much the optimal profiles move and morph depending on the Reynolds number. At low Re the suction profiles are narrowly spread and positioned near the leading edge of the cylinder. As Re increases, the profile spreads out and moves further leeward on the cylinder. This shift can be seen in Figure 6 where a sample of the results at different Re are shown for the moving distribution control. In addition, lines marking the uncontrolled separation angle and the angle of suction are shown for each profile. Evidently, there is a relationship between the suction angle, θ_q , and the Reynolds number, and by extension the uncontrolled separation angle also. Figure 7 (a) and (b) plot these relationships respectively.

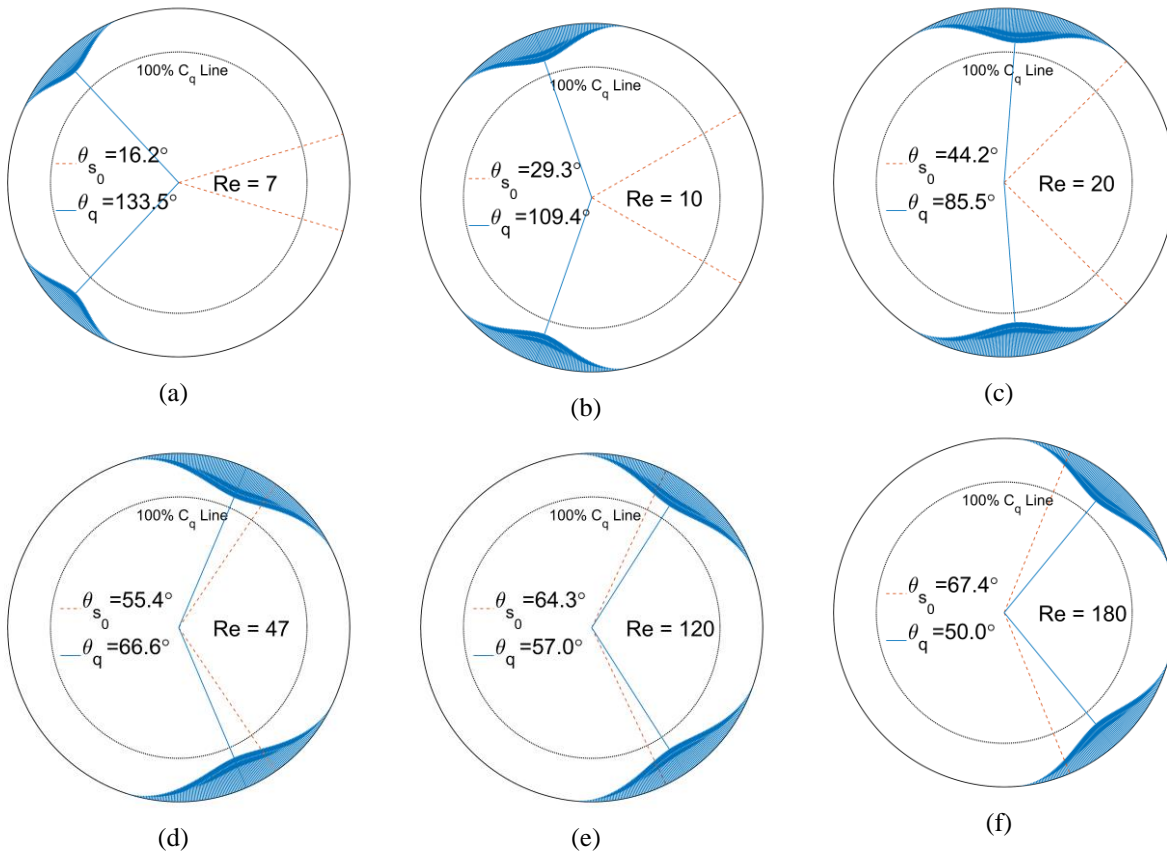


Figure 6: Variations in optimal suction profiles for moving distribution control at various Re . The inner dotted circle marks where the local suction coefficient is 100, i.e. $v_w = U$. The uncontrolled (initial) separation angle, θ_{s_0} , and resulting centre of suction, θ_q , are also plotted and their values displayed.

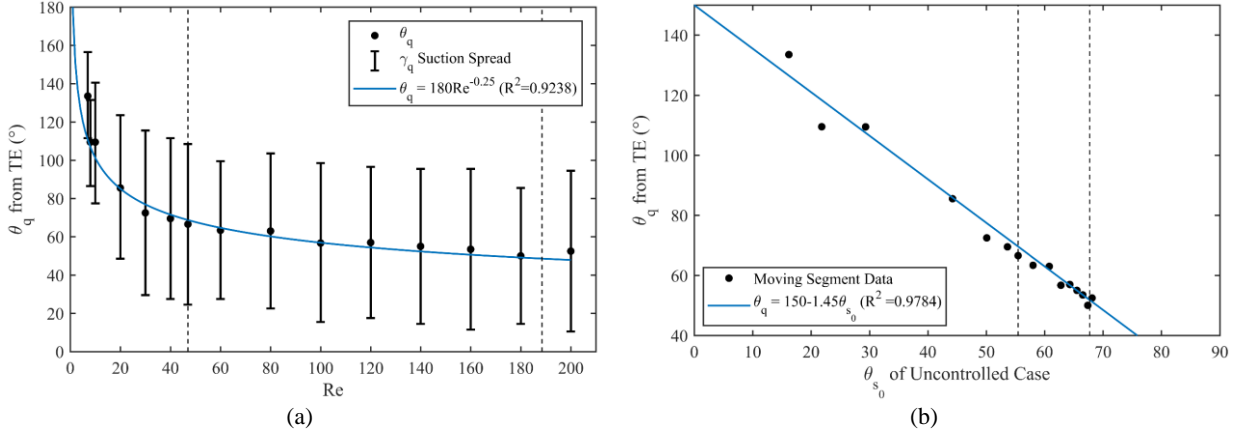


Figure 7: How the non-uniform suction profile with moving distribution control moves with (a) Reynolds number and (b) initial separation angle. The vertical lines mark the regime changes of the uncontrolled flow.

From this figure, it is clear that there is a strong relationship between Re , θ_{s_0} and θ_q . Similar discussion can be made about these relations as for C_q in the earlier section. These points will not be repeated beyond stating that the results confirm a dependence on the Reynolds number and on the uncontrolled separation angle for the application of suction control; that it is not constant at all Re ; and that it would be of interest to see if these results could be extended to higher Re . There appears to be less correlation with the spread of suction, γ_q , however, which has an average value of 75° .

C. Effect on drag

The aerodynamic characteristics of the cylinder were of particular interest in this study, so the drag components for the optimally controlled cases were measured. These are plotted in Figure 8 alongside the values for the uncontrolled case using the relationships taken from the numerical analysis by Henderson²⁴. There are several features to note here, in particular: the general trend of the total drag, C_{d_t} , and the behaviour of its two components, C_{d_f} & C_{d_p} .

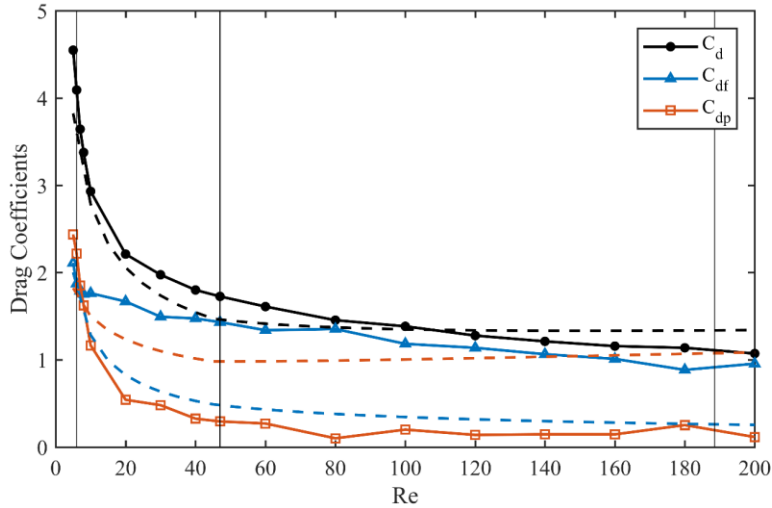


Figure 8: Drag components for the optimally controlled (solid lines) and uncontrolled (dashed lines) flows. The vertical lines delineate the uncontrolled flow regime changes.

Figure 8 shows that all the values follow similar trends to the uncontrolled case: beginning very high and decreasing with a power-law relationship with increasing Re . However, where one might have expected the elimination of boundary layer separation to improve the drag, it is evident that this is not always the case. For all $Re <$

100, the drag is worse for the controlled case than the uncontrolled case; only above $Re = 100$ is improvement seen. The explanation for this behaviour can be found by analysing the components of the drag, shown in the same figure.

The first thing to note is the shift in pressure drag. Since the pressure drag is predominately contributed to by the loss of momentum to the boundary layer and the vortices that form in the separated region, one might have expected the pressure drag to be eliminated entirely, along with the boundary layer separation. This is clearly not the case. The optimisation studies searched for control parameters that eliminated separation with minimal suction effort, therefore the boundary layer is not entirely removed. With this objective, despite θ_s being successfully reduced to zero, momentum from upstream is still lost to the boundary layer, so the pressure is not fully recovered over the leeward side. This can be seen visually by the slow velocity region in the wakes of the controlled flows in Figure 4. Nevertheless, the pressure drag is substantially reduced, particularly in the vortex shedding regime.

Counteracting the improvement of this one component, is a worsening of the other: the skin friction drag. With the removal of the separated region of flow, the boundary layer has a higher velocity across the entire surface of the cylinder, as was highlighted by the increased velocity vectors in Figure 4. This higher boundary layer velocity results in a stronger shear force and, correspondingly, a greater skin friction drag. At low Re , where the viscous effects of the flow are more important, this increase in skin friction drag can overwhelm the improvement in pressure drag to result in a worsening of the total drag. In this case, for the objective of eliminating separation using moving distribution control, this occurs for all $Re < 100$. Only above $Re = 100$, where the inertial effects are sufficiently dominant and the improvement in pressure drag is more substantial, does the control work in the favour of reducing total drag. This balance of drag components will be discussed to further depth in the section on drag objectives.

D. Pressure profiles

To complete the analysis of the controlled flow behaviour and characteristics, the pressure coefficient profiles are provided in Figure 9. In the first plot, Figure 9 (a), the time-averaged pressure coefficients for the uncontrolled flow are compared to values from experiments in the literature. These values, labelled ‘Zdravkovich’, in the plot are taken from experimental values from Thom²⁷, and Homann²⁸ in the Re range $36 < Re < 107$ and compiled by Zdravkovich in his textbook². Hence, why at low Re values, $Re \leq 20$, the pressure coefficients are seen to differ quite substantially. At none of the investigated Re values does the leading edge pressure coefficient equal unity as determined by potential flow theory, however it does trend towards that value with increasing Re . It is common in the literature to approximate the location of the separation point as corresponding to the inflection point on the pressure profile^{5,6}. Looking at this figure, it can be seen that the inflection point roughly corresponds with the measured θ_s though not always, as with $Re = 4$.

In Figure 9 (b), the controlled flow is compared to the uncontrolled flow for $Re > 40$. There are several features to highlight here. Firstly, the pressure profile of the controlled flow fills out more to become similar to the profile given by potential flow theory. The minimum pressure coefficient is much lower, though, with values between -3.75 and -4.5. This is similar to what was seen in the experiments by Pankhurst and Thwaites¹⁷. The lower pressure coefficient likely arises due to the flow being accelerated more than it would in the inviscid case, as the suction removes the low momentum particles and providing a pressure gradient to entrain higher velocity free-stream particles, accelerating them as they replenish the boundary layer. In addition, as the flow is no longer inhibited by the separated region, the pressure at the leading edge moves closer to $C_p = 1$. Finally, it is important to note that the plateau of C_p near the trailing edge is not eradicated – momentum is still lost to the boundary layer.

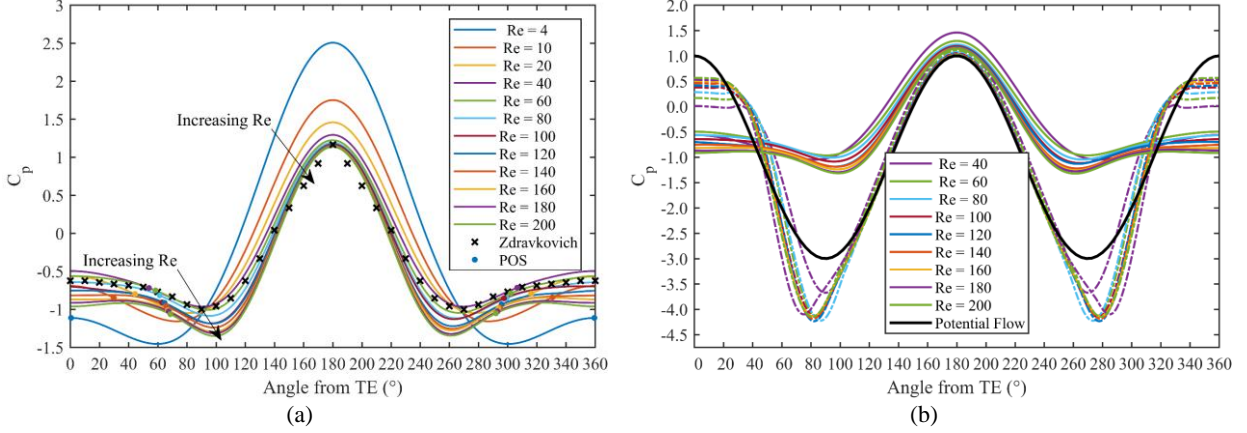


Figure 9: Pressure coefficient profiles over surface of cylinder for (a) uncontrolled case, and (b) both uncontrolled (solid line) and controlled (dot-dashed line) cases.

C_{d_t} and C_{d_p} objectives

So far, we have investigated the optimal control for eliminating separation on the circular cylinder. As has been discussed earlier, however, much of the present literature is more concerned with the vortex shedding and drag coefficients than the boundary layer behaviour. Now, we consider the effect of changing the objective of the optimisation, to minimise the total drag or pressure drag using the moving distribution control method.

A. Comparison with θ_s objective

Figure 10 below shows the resulting flow fields at $Re = 120$ for the optimal control found for each objective using the moving distribution method. It is clear from this figure that the control required to achieve each objective differs significantly, as does the behaviour of the resulting flow. While the uncontrolled flow figure was taken from a time-dependent simulation, the other figures were taken from the final stage of the optimisation process and thus with a steady-state condition. Naturally, the steady-state flows are symmetrical, therefore, and there are no lateral movements in the wake as with the uncontrolled flow.

The first feature to note in Figure 10 is the difference in suction profiles for each optimum control. As was shown earlier, the suction to eliminate separation at $Re = 120$ was spread wide and focussed near the trailing edge, with a relationship close to $\theta_q = 180 Re^{-0.25}$. The suction profiles for the drag objectives are narrower and closer to the top and bottom of the cylinder (90° and 270°). It can be seen visually, that the amount of suction, C_q , is much smaller for these objectives also – particularly for the total drag objective in Figure 10 (c). This makes sense given what the earlier results revealed about the balance of drag components: while boundary layer suction can reduce the pressure drag, it comes at the cost of increasing the skin friction drag. The separation angle objective often resulted in a net increase in drag because the suction was too strong, so it is appropriate that the optimal suction profile to minimise total drag employs less suction. This balance can be observed in the velocity vectors near the wall for the separation objective and the total drag objective. For the former, the vectors are concentrated and large, whereas for the total drag control a more balanced profile is observed.

The resulting flow fields for each objective differ significantly. The most obvious feature is the wake size – both its length and width. The wake in these figures can be considered the paler blue region centred on the trailing edge, bordered by the dark blue lines where the flow is stagnant. This delineates the two shear layers of reversed flow in the wake, and forward flow outside. With this definition, the separation objective flow in Figure 10 (b) has no real wake as it has no reversed flow, only stagnant fluid. On the other hand, the total drag objective has the longest wake. The pressure drag objective is about halfway between in terms of length, but has a similar wake-width to that for the C_{d_t} objective – a separation angle corresponding to about 45° from the trailing edge.

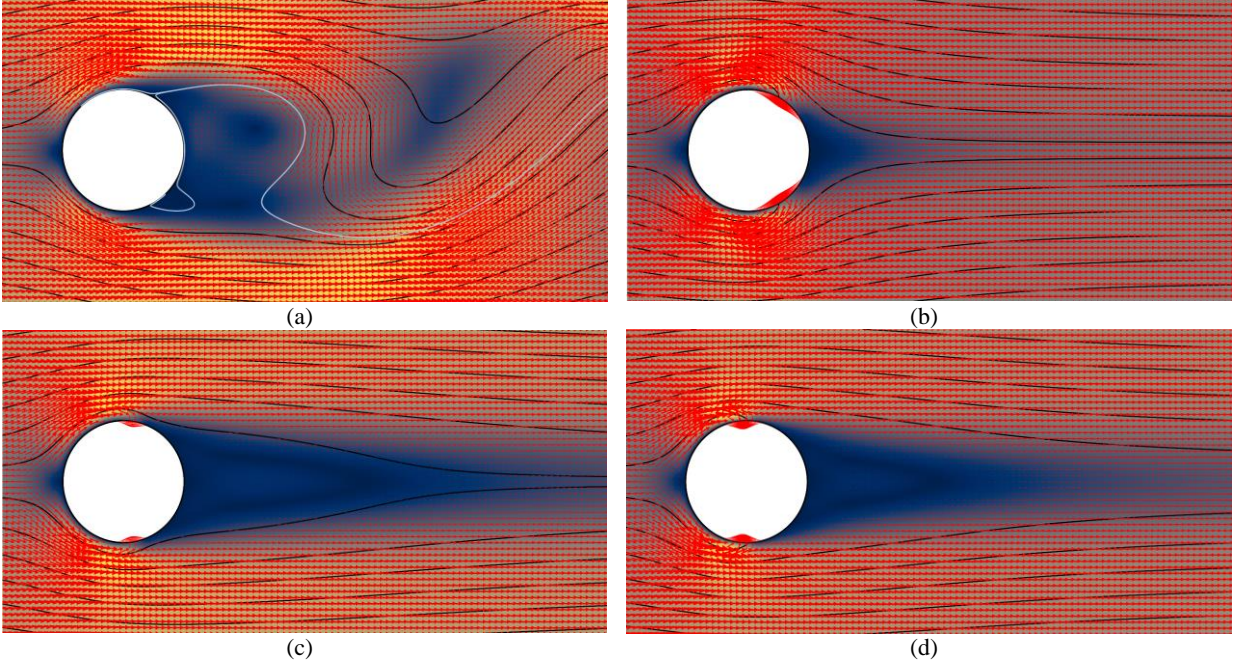


Figure 10: Instantaneous flow field at $Re = 120$ showing velocity vectors and surfaces, as well as streamlines from the inlet for the (a) uncontrolled case, and controlled for minimising (b) separation angle, (c) total drag and (d) pressure drag objectives.

Figure 11 shows how the optimal control differs depending on the objective of the optimisation. The amount of suction and the location of suction are plotted against the Reynolds number, as in Figure 5 and Figure 7. As with the θ_s objective, clear trends can be seen in the optimal control parameters for the other objectives. Contrary to the trend seen for minimising θ_s , however, Figure 11 (a) shows that the amount of suction required to achieve the drag objectives decreases with increasing Re in all flow regimes. This figure also shows a levelling off at $C_q = 5$ for the amount of suction to minimise total drag within the vortex shedding regime.

Figure 11 (b) shows that the location of optimal suction for the drag objectives follows a similar trend to that for the separation angle. A power law is seen for each, and approximate fits are given in the legend of that figure. These fits have been rounded, so are not necessarily the best fits for the data, but help to make comparisons easier. It can be seen that the drag objectives result in suction profiles located closer to the leading edge, and begins to level off near 90° . This fits with what Kim and Choi¹⁹ found for $Re = 100$, with the drag on a cylinder improving most by slot suction and blowing when the slots were located between 80° and 100° . The data for the pressure drag objective is more scattered here.

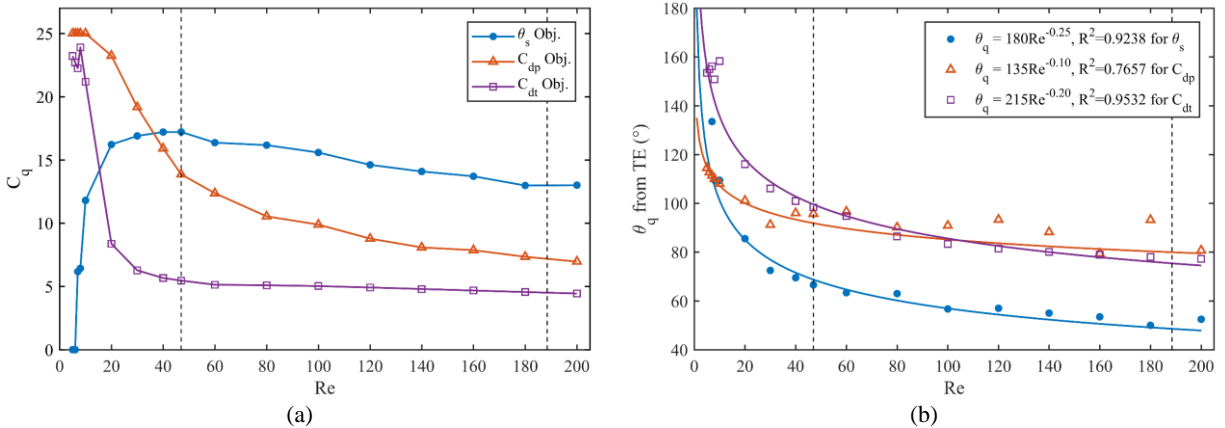


Figure 11: Effect of objective on optimal suction characteristics: (a) the amount of suction, and (b) the location of suction.

In addition to the control characteristics, the features of the resulting flow are of equal interest. Since the drag objectives result in optimally controlled flows that still have boundary layer separation, Figure 12 shows the separation angle for each controlled case in comparison to the time-averaged value for the uncontrolled case taken from Wu et al⁷. Again, we see a levelling off of the data for the total drag objective. Here the separation angle plateaus near the 45° mark, thus the difference in separation angle to the uncontrolled case increases in the vortex shedding regime. This suggests that in the vortex shedding regime there is a particular optimal control case that scales appropriately with the changes that occur as Re increases in this region. The 45° mark may bear some significance as the location at which the separation is restrained to by the optimal control for C_{dt} .

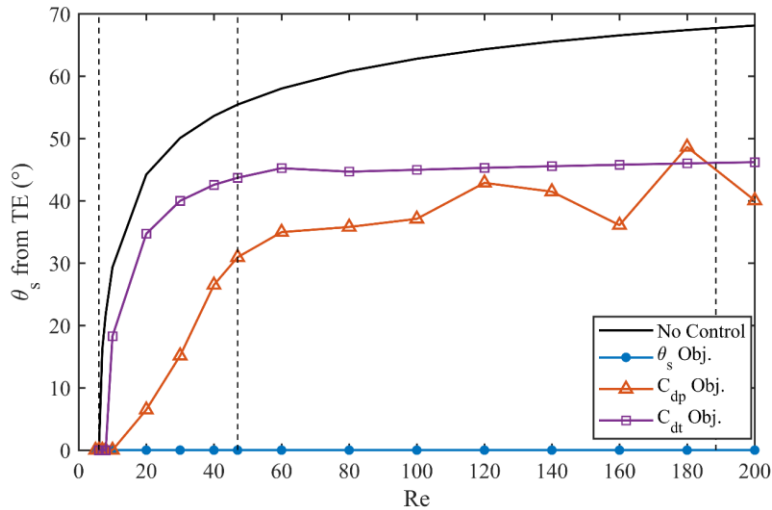


Figure 12: Separation angle for the optimally controlled flow for each objective.

B. Drag components

The effect of control on the components of drag is of great interest for these objectives, particularly how the skin friction and pressure drag changes are balanced to achieve the minimum possible total drag. The total drag of the optimally controlled flows using the moving distribution control method are displayed in Figure 13. Here, the relationships from Henderson²⁴ are also plotted for comparison to the uncontrolled case.

From this figure, it can be seen that the improvement to drag is much more substantial for these objectives than when eliminating separation – particularly in the vortex shedding regime. Before the von Karman street begins forming at $Re = 47$, there is little improvement in the total drag from either the C_{dt} or C_{dp} objectives. Whereas the separation objective in many instances resulted in a worsened total drag coefficient, the C_{dt} objective resulted in controlled flows that were in no case worse than the uncontrolled flow. On the surface this is unsurprising, as the optimisation algorithm would return zeroed control parameters if no suction setup could improve upon the uncontrolled flow – thus the total drag should never be higher than the uncontrolled case for this objective – however, as can be seen in Figure 11 and Figure 12, the optimal flow was achieved with significant control applied in every instance. This shows that the drag can always be improved, or at least matched, by the application of suction control in the entire investigated Reynolds range. It also suggests that very different control parameters may result in flows with near-identical macroscale features. The C_{dp} objective, on the other hand, had slightly worse drag characteristics in the unseparated and vortex pair regimes. This fits with what was learned from the separation objective results.

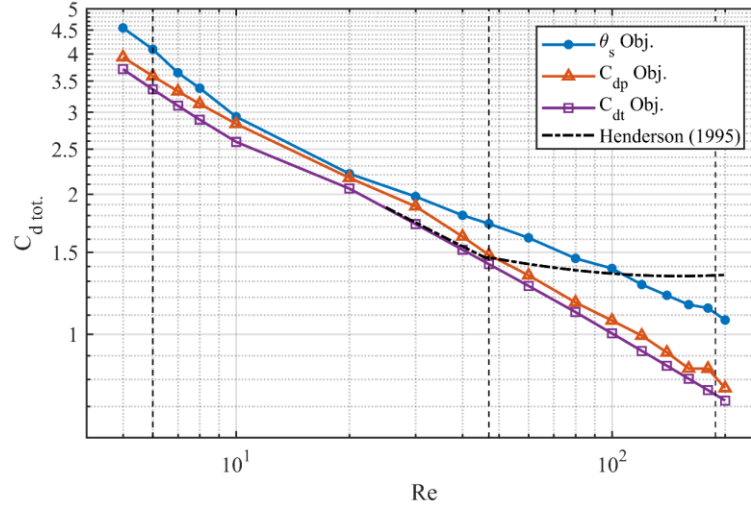


Figure 13: Total drag of the optimally controlled cases compared with the time-averaged value for the uncontrolled flow.

The particularly important result shown in Figure 13 is the vast improvement in drag that occurs in the vortex shedding regime. Here, where the uncontrolled drag line begins to curve upwards, the drag-optimised cylinder characteristics to decrease at the same rate as in the vortex-pair regime. This means that, once vortex shedding has begun, as Re continues to increase, the maximum improvement in drag will also increase. This bodes well for practical implementations, as typical engineering scenarios of bluff body flow occur at much higher Re . It is interesting that the characteristics for the total drag objective continue along the same trend as the ‘subcritical’ uncontrolled flow (subcritical here meaning before the onset of vortex shedding, $Re < 47$). Bearing in mind that the results for the C_{dt} objective represent the best possible improvement in drag (at least using suction control), this suggests some physical significance about the flow. The transition from steady separated flow to transient vortex shedding has a big impact on the aerodynamic characteristics of the uncontrolled cylinder: the pressure drag stops decreasing with Re and begins to increase, though the skin friction drag coefficient continues to decrease at near its prior rate, resulting in the curved C_{dt} profile in the range $47 < Re < 188.5$. The fact that the optimally controlled flow is unaffected by this transition, and the total drag continues to decrease at its prior rate, suggests that the significant change imposed by the control is the elimination of vortex shedding – and therefore, that the elimination of vortex shedding provides the maximum possible improvement in drag. This would be an important finding, because much of the literature regarding the control of flow around a circular cylinder has already been focussed on the elimination of vortex shedding (typically because of the detrimental lateral forces), or separately on minimising the total drag. If the present hypothesis is correct, and the best drag reduction is achieved by the elimination of vortex shedding alone, then this would go some way in connecting the findings in the literature and helping to clarify the best aims for potential flow control methods.

Figure 14 goes some way to verifying this hypothesis. In this figure three sources of data are shown for each of the drag components: the actual drag coefficients for the uncontrolled flow (dashed lines), the drag coefficients for the uncontrolled flow with the *subcritical trend continued into the vortex shedding regime* (dotted lines), and finally the results of the optimally controlled flow from the present study (solid lines). In addition, some manipulation to the data has been performed. As before, the suction control resulted in a decrease in pressure drag and an increase in skin friction drag. To test the vortex shedding hypothesis, the pressure drag curve was shifted up 0.38 to line up with the uncontrolled value at the regime change, correspondingly the skin friction curve was shifted down an equal amount. The total drag curve was not shifted.

This figure has many interesting features. First of all, the dramatic improvement on total drag by the optimal non-uniform suction is more evident on this standard grid. Here it can be seen that it is not only substantially improved compared to the uncontrolled cylinder, but it is even better than for a cylinder with the subcritical trend continued. The second important feature, is the alignment of the pressure drag coefficient. This characteristic lines up almost perfectly with the extended subcritical relationship. It is reasonable to consider the rise in pressure drag of the uncontrolled cylinder to be due entirely to the onset of dynamic vortex shedding, therefore these results suggest that the absolute best characteristics that can be achieved are those that minimally eliminate vortex shedding. The characteristics defined by the dotted lines in this figure could be considered to be those of an idealised cylinder that,

through extreme smoothness or some other mechanism, is somehow able to maintain steady flow in the vortex shedding regime, i.e. the instability jump to vortex shedding never occurs as Re is increased on the cylinder. Fornberg^{29–31} has long highlighted the importance of the ‘steady though unstable’ cylinder in typically unsteady regions as a potential aim for flow control. Here we see that it may represent the optimal controlled flow for minimising drag – at least for control by boundary layer suction. The optimal flow achieved with non-uniform suction control here is even better than this idealised cylinder. The skin friction drag coefficient comes in under both uncontrolled cylinder characteristics, hence why the total drag is improved even beyond the subcritical trend. This may be due to the non-uniform suction minimising the increase in skin friction by only accelerating the boundary layer over a portion of the surface, rather than the entirety as the idealised cylinder would encounter.

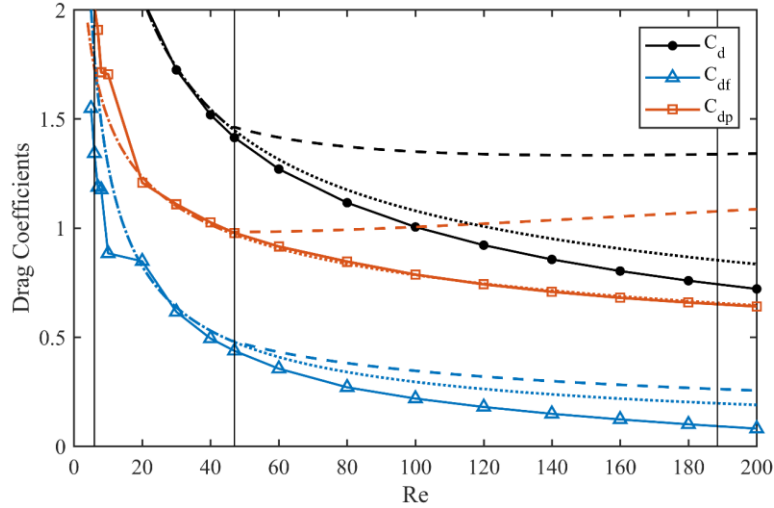


Figure 14: Drag components for optimally controlled flow with total drag objective, J_2 . Note, C_{dp} and C_{df} have been shifted up and down 0.38 respectively. Here the characteristics are shown for the present total drag-optimised results (solid lines), uncontrolled cylinder (dashed lines), and the extended sub-critical trends (dotted lines). The vertical lines mark the regime changes for the uncontrolled flow.

Verification by time-dependent studies

One of the major limiting factors of the optimisation procedure in this study was the use of steady-state solvers for flows that, when not appropriately controlled, are unsteady. To test the validity of the assumptions in the optimisation process, time-dependent studies were performed with the optimal control found for each objective at $Re = 60$ and $Re = 180$ – testing the two extremes of the 2D vortex shedding regime. The key results of these studies are shown in Figure 15 below, along with the steady-state results which are plotted as markers on the right vertical of the grid. In each case, the vortex shedding was allowed to fully develop on the uncontrolled cylinder, before the control was ramped up from 0% to 100% of its strength in a linear fashion over the course of $t = 5T$, where T is the period of vortex shedding given by Roshko’s equation $St = \frac{D}{TU} = 0.212 - \frac{4.5}{Re}$. The controlled flow was then allowed to fully develop. The time was non-dimensionalised according to $t^* = t \frac{U}{x_0}$, where x_0 is the distance from inlet to the centre of the cylinder (see Figure 1).

Figure 15 shows the results of these verification studies, with the steady-state results shown as markers on the right vertical axis. As can be seen in Figure 15, the results actually fit quite well between the time-dependent and steady-state controlled results. However, it is evident for the results at $Re = 180$, the assumption that the optimally controlled flows are steady was incorrect for the C_{dt} and C_{dp} objectives as anticipated. In Figure 15 (b) it can be seen by the oscillation of the separation angles on the upper and lower surfaces that the flow is not steady. Vortex shedding has not been eliminated as was hypothesised earlier. Despite the assumption breaking down here, the steady-state results still predict the actual values reasonably well as shown by the agreement to the final time-step. Even for the oscillating separation angles, the steady-state result gives the maximum separation angle for the uncontrolled case. The drag

values are mostly accurate also, underestimating the values for the C_{dt} objective only slightly, as was shown to be the behaviour for the steady-state approximations in Figure 3 (b). The only values that are significantly inaccurate are those for the drag components for minimising pressure drag at $Re = 180$. This can be seen in Figure 15 (d), where the pressure drag and skin friction drag components are underestimated, resulting in the steady-state total drag being lower than the reality by 0.106 (-3.29%).

In addition to some of the transient details being missed in the steady-state simulations, another feature was absent for the flow at $Re = 60$ with the C_{dt} objective control applied. That feature is a small separation bubble which formed where the suction was applied in the time-dependent study. The impact of this can be seen in Figure 15 (a) where the separation angle was detected first at 93.39° where the separation bubble formed. This bubble was very small, as can be seen in the inset of this figure, and had no significant impact on the flow and the later major separation point (which is also plotted on this figure). It does highlight, however, that making the assumption of steady-state flow presents some risk of small or transient features being missed. In the bigger picture, though, the steady-state optimisation process achieved valuable results with much smaller time requirements for the simulations. The major characteristics of the flow were accurately modelled.

It is safe to say, therefore that the results from the steady-state optimisation studies are sufficiently accurate to be relied upon in this Reynolds range – particularly, when only concerned with the general behaviour of the flow: the aerodynamic characteristics, the separation point, etc. The steady-state studies failed to show transient behaviour in the flow, such as the oscillation of the near wake and vortex shedding in the far wake. This verification by time-dependent studies validates the key results of the optimally controlled flows, but does not necessarily confirm that they are the optimum. Such a validation would require full parametric studies of transient flows that makes it computationally prohibitive. For these results, the optimal control for the separation angle objective can be considered correct, while the optimal controls for the other objectives may be assumed to be true, with some caution.

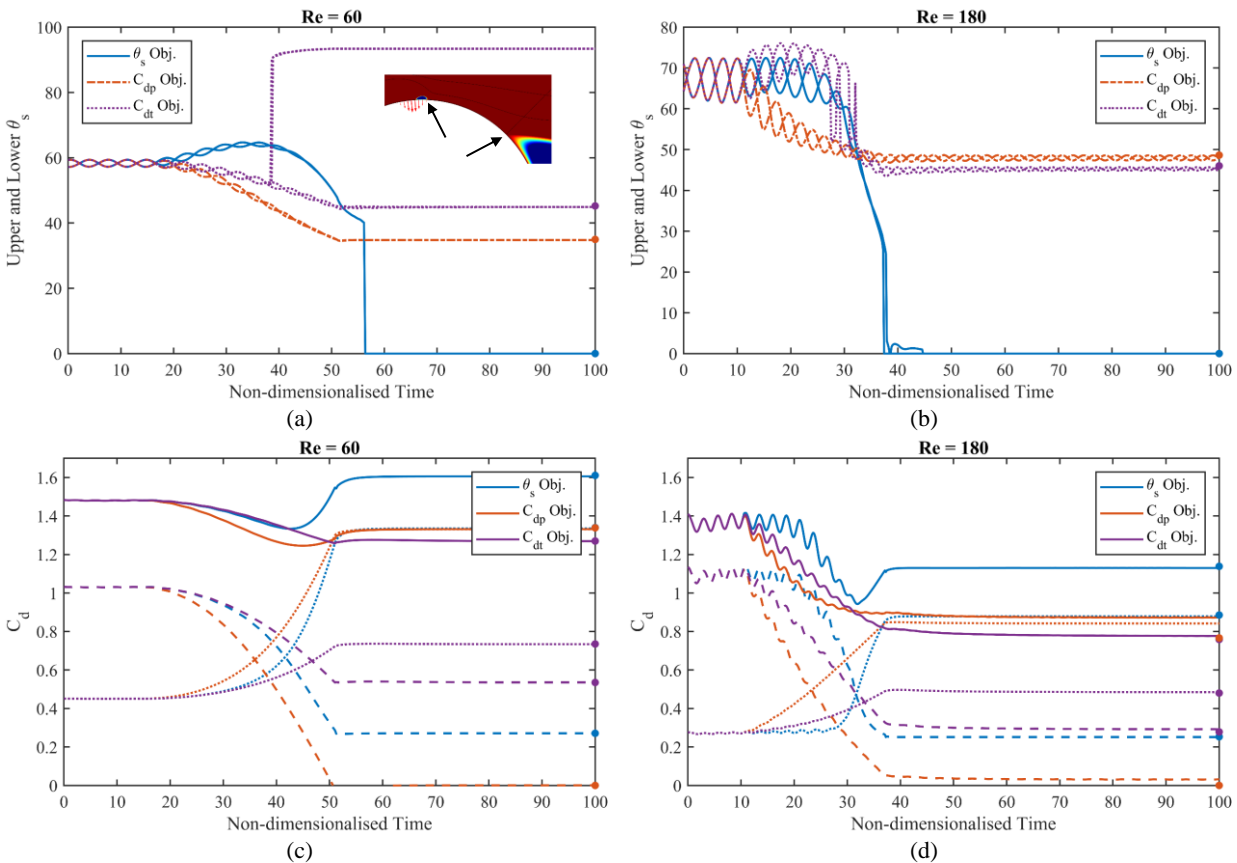


Figure 15: Results from time-dependent studies of the optimum moving distribution control for each objective, showing (a-b) the instantaneous separation angles, and (c-d) the drag components. Inset on (a) is a tangential velocity surface for the C_{dt} objective at $Re = 60$ showing the separation bubble and main separation, that give rise to two sets of measurement for θ_s .

CONCLUDING REMARKS

In this study, we have presented a method for determining the optimum control parameters of boundary layer suction in an effort to achieve a variety of objectives for the flow around a circular cylinder: eliminating separation, θ_s , minimising total drag, C_{d_t} , and minimising pressure drag C_{d_p} . Numerical simulations were performed on the flow around a circular cylinder in the Reynolds range $4 < Re < 200$, and optimisation algorithms were used to determine the best parameters for the control. To thoroughly investigate the numerous potential applications of non-uniform suction, several models were tested. The moving distribution – a suction distribution with compact support and single locus – proved to be superior. It provided efficient control, while being simple to implement and achieve optimality. The results of this study provide a variety of insights into the problem of flow around a circular cylinder and flow control generally.

Firstly, the approach of carrying out optimisation processes on unsteady flow using a steady-state approximation provided results that were sufficiently accurate while enabling wide-ranging simulations to be carried out in far less time than corresponding time-dependent simulations. This approach may be applied at higher Reynolds numbers for this flow – or for other types of external and internal flow – with the caveat that at higher Re , where more of the flow becomes unsteady and turbulent, its reliability will likely be diminished. The assumption that the optimally controlled flow will be steady holds less well for objectives not directly related to vortex shedding (as seen by the C_{d_t} and C_{d_p} objective results), but can likely be as successfully employed for parameters directly related to the unsteady aspects of the flow (e.g. the lift coefficient or certain vorticity measures) as for the separation angle parameter used in the present study.

Secondly, clear relationships have been derived between characteristics of the uncontrolled flow and the optimal control for a variety of important objectives. The substantial improvement in efficiency of non-uniform suction in comparison to uniform suction, suggest this is the best form of boundary layer suction control. However, the dependency of its location on the parameters of the flow may make it impractical in many circumstances. Since C_q and θ_q change with predictable trends though, such as $\theta_q = 180 Re^{-0.25}$ for the θ_s objective, this issue may be mitigated.

Another important finding was the balance of drag components in the suction-controlled flows. Eliminating separation did not always reduce the total drag because the skin friction component is increased due to the fuller boundary layer profile. Above $Re = 100$, however, the controlled attached flow has a reduced drag as skin friction becomes less significant. It may be reasonably expected that for all $Re > 100$, if separation is prevented by optimal suction control, the total drag will be reduced. The controlled flow with minimised total drag almost always required less suction, in order to balance the pressure and skin friction drag components. The drag-optimised flows followed trends similar to that seen for a cylinder with steady flow in the unsteady regime (steady, unstable flows as described by Fornberg³¹). The pressure drag component followed almost the same relationship with Re as an idealised steady flow, but shifted down due to the delayed separation – the total drag was similar. This may present an opportunity for a computationally cheap method for predicting the maximum potential improvement in drag that optimum suction control can provide – simply evaluating the flow in question with the steady Navier-Stokes equations.

Finally, the investigation into the importance of the separation angle, both as an uncontrolled parameter of the flow and as an objective of control, has yielded valuable results. It has been determined that the relationships between the flow and the optimal control could equally be expressed as a relationship with θ_{s_0} than with Re . In many cases this results in less convoluted connections; the $\theta_q - \theta_{s_0}$ relationship was linear, even. This may have the advantage of making it easier to apply the lessons of optimal control in one flow regime to another – or indeed to flows with bodies of totally different shapes. Less dependence on the initial separation angle was seen for the drag objectives, however it plays a significant role as an outcome of the controlled flows, as seen by the repeated $\theta_s = 45^\circ$ for the drag-optimised flows.

The outcomes found here improve the current understanding of the control of flow around bluff bodies – and separated flows generally – with the importance of the separation angle and the relationships of the drag components seen to be significant. These results, and the methods used to obtain them, bear great promise for application in broader Reynolds ranges or for different types of flow, and provide a potential method for economically estimating the lowest possible drag by boundary layer suction control.

ACKNOWLEDGMENTS

REFERENCES

1. Williamson, C. H. K. 'Vortex Dynamics in the Cylinder Wake'. *Annu. Rev. Fluid Mech.* **28**, 477–539 (1996).
2. Zdravkovich, M. M. *Flow Around Circular Cylinders*. (Oxford University Press Inc., 1997).
3. Thompson, M. C. & Hourigan, K. 'The shear-layer instability of a circular cylinder wake'. *Phys. Fluids* **17**, 21702 (2005).
4. White, F. M. *Fluid Mechanics (7th Edition)*. (McGraw Hill, 1986). doi:10.1017/CBO9780511794353
5. Weidman, P. D. 'Wake transition and blockage effects on cylinder base pressures'. (California Institute of Technology, 1968).
6. Achenbach, E. 'Distribution of local pressure and skin friction around a circular cylinder in cross-flow up to $Re = 5 \times 10^6$ '. *J. Fluid Mech.* **34**, 625–639 (1968).
7. Wu, M.-H., Wen, C.-Y., Yen, R.-H. & Weng, M.-C. 'Experimental and numerical study of the separation angle for flow around a circular cylinder at low Reynolds number'. *J. Fluid Mech.* **515**, 233–260 (2004).
8. Fransson, J. H. M., Konieczny, P. & Alfredsson, P. H. 'Flow around a porous cylinder subject to continuous suction or blowing'. *J. Fluids Struct.* **19**, 1031–1048 (2004).
9. Kwon, K. & Choi, H. 'Control of laminar vortex shedding behind a circular cylinder using splitter plates'. *Phys. Fluids* **8**, 479–486 (1996).
10. Scruton, C. & Walshe, D. E. J. 'A means for avoiding wind-excited oscillations of structures with circular or nearly circular cross section'. *Natl. Phys. Lab. (UK), Aero Rep.* **335**, (1957).
11. Sung, Y., Kim, W., Mungal, M. G. & Cappelli, M. A. 'Aerodynamic modification of flow over bluff objects by plasma actuation'. *Exp. Fluids* **41**, 479–486 (2006).
12. Rashidi, S., Dehghan, M., Ellahi, R., Riaz, M. & Jamal-Abad, M. T. 'Study of stream wise transverse magnetic fluid flow with heat transfer around an obstacle embedded in a porous medium'. *J. Magn. Magn. Mater.* **378**, 128–137 (2015).
13. Choi, H., Jeon, W.-P. & Kim, J. 'Control of Flow Over a Bluff Body'. *Annu. Rev. Fluid Mech.* **40**, 113–139 (2008).

14. Rashidi, S., Hayatdavoodi, M. & Esfahani, J. A. 'Vortex shedding suppression and wake control: A review'. *Ocean Eng.* **126**, 57–80 (2016).
15. Schlichting, H. *Boundary-Layer Theory (7th Edition)*. (McGraw-Hill, 1987).
16. Multiple Authors. *Boundary layer and flow control: its principles and application*. (Pergamon Press, 1961).
17. Pankhurst, R. C., Thwaites, B. & Walker, W. S. *Experiments on the Flow Past a Porous Circular Cylinder Fitted with a Thwaites Flap*. **2787**, (HM Stationery Office, 1953).
18. Hurley, D. G. & Thwaites, B. *An experimental investigation of the boundary layer on a porous circular cylinder. Aeronautical Research Council Reports and Memoranda* **2829**, (1951).
19. Kim, J. & Choi, H. 'Distributed forcing of flow over a circular cylinder'. *Phys. Fluids* **17**, 33103–33116 (2005).
20. Min, C. & Choi, H. 'Suboptimal feedback control of vortex shedding at low Reynolds numbers'. *J. Fluid Mech.* **401**, 123–156 (1999).
21. Boujo, E., Fani, A. & Gallaire, F. 'Second-order sensitivity in the cylinder wake: optimal spanwise-periodic wall actuation and wall deformation'. *arXiv Prepr. arXiv1808.02796* (2018).
22. Conn, A. R., Scheinberg, K. & Vicente, L. N. *Introduction to derivative-free optimization*. **8**, (Siam, 2009).
23. Tritton, D. J. 'Experiments on the flow past a circular cylinder at low Reynolds numbers'. *J. Fluid Mech.* **6**, 547–567 (1959).
24. Henderson, R. D. 'Details of the drag curve near the onset of vortex shedding'. *Phys. Fluids* **7**, 2102–2104 (1995).
25. Wieselsberger, C. 'New data on the laws of fluid resistance'. *Phys. Zeitschrift* **22**, (1922).
26. Powell, M. J. D. 'The BOBYQA algorithm for bound constrained optimization without derivatives'. *Cambridge NA Rep. NA2009/06, Univ. Cambridge, Cambridge* 26–46 (2009).
27. Thom, A. & Ingram, T. G. 'The flow past circular cylinders at low speeds'. *Proc. R. Soc.* **141**, 651–669 (1933).
28. Homann, F. 'Influence of higher viscosity on flow around cylinder'. *Forsch. aus dem Gebiete des Ingenieurwes.* **17**, 1–10 (1936).
29. Fornberg, B. 'A numerical study of steady viscous flow past a circular cylinder'. *J. Fluid Mech.* **98**, 819–855 (1980).

30. Fornberg, B. 'Steady viscous flow past a circular cylinder up to reynolds number 600'. *J. Comput. Phys.* **61**, 297–320 (1985).
31. Fornberg, B. & Elcrat, A. R. 'Some observations regarding steady laminar flows past bluff bodies'. *Philos. Trans. R. Soc. A Math. Phys. Eng. Sci.* **372**, 115–134 (2014).